IMPROVING THE DETECTION CAPABILITY OF SPATIAL FAILURE MODES USING DOWNWARD-LOOKING SENSORS IN TERRAIN DATABASE INTEGRITY MONITORS

Ananth Vadlamani and Maarten Uijt de Haag
Ohio University, Athens, Ohio

Abstract

This paper discusses various methods of improving the detection capability of horizontal and vertical failure modes for a terrain database integrity monitor that is purely based on the inputs from downward looking sensors. Terrain database integrity monitors which use radar altimeter and GPS inputs have previously been proposed for Synthetic Vision Systems (SVS). An SVS provides pilots with either a Heads Down Display (HDD) or a Heads Up Display (HUD) containing aircraft state, guidance and navigation information, and a virtual depiction of the terrain as viewed "from the cockpit". The source used to generate the terrain depicted on these displays is a Digital Elevation Model (DEM). Due to the compelling nature of the displays, it is quite possible for the pilots to use the display for functions other than its original intended function. It may be hard to avoid such a scenario, especially if the system is certified as an advisory system. When using SVS display technology for functions other than advisory it may be necessary to include a DEM integrity monitor whose performance is specified by probabilities of Missed Detection, Fault–Free Detection and Time-to-Alarm. Ideally, the DEM represents the height or elevation of the terrain at corresponding coordinates (e.g. latitude and longitude) expressed in a predefined vertical datum. However, the given elevations deviate from the true elevations due to systematic and blunder errors that are present in the DEM primarily due to the way in which they are generated from different sensor technologies such as photogrammetry, remote sensing, etc. and the manual post-processing process. Another source of error of lesser significance is the flat earth approximation over relatively larger areas, while collecting the data. The described integrity monitor method is based on the comparison of the DEM terrain profile with an independent terrain profile synthesized from a downward looking sensor (Radar Altimeter) and GPS-Wide Area Augmentation System (WAAS) measurements. Due to the inherent presence of sensor measurement noise and random errors in the DEM, it is not possible to detect vertical biases and horizontal translations in the DEMs in an absolute sense, but only in a statistical manner. When considering the probability of missed detection, a region of uncertainty can be defined as the geo-spatial region that contains the set of all possible aircraft positions surrounding the true position which do not result in an integrity alarm, given the presence of a DEM failure. The integrity monitor's capability to detect horizontal failure modes is directly related to the extent of the uncertainty or missed detection region; the smaller the region, the better the integrity monitor is capable of detecting a horizontal failure. A method is proposed to detect horizontal failures, which monitors the Kalman filter's covariance matrix over the region of uncertainty. A similar concept as that used for integrity monitoring has been explored for its potential applications in terrain navigation. Flight test data from NASA's flight trials at Eagle/Vail (EGE), Colorado and Ohio University's flight trials in Juneau (JNU), Alaska is used to evaluate the performance of the proposed methods.

Introduction

Take-off and landing are difficult phases of a flight but in addition another very difficult situation faced by pilots is when they cannot see anything of the environment outside of the cockpit. These zero visibility situations can occur due to bad weather conditions like clouds, rain, fog, snow or darkness that reduce the number of visual cues and potentially result in loss of spatial orientation. Continuing on a safe flight and landing the aircraft while experiencing spatial disorientation can become extremely tricky. Even though most aircrafts are equipped with instruments to aid the pilot during flight in Instrument Meteorological

Conditions (IMC), statistics disclosed by a Flight Safety Foundation revealed that 41% of all aircraft accidents occurred when the pilot flew into terrain while in full control of the aircraft and crashed the aircraft while traversing particularly rough terrain like hills and mountains. This is referred to as Controlled Flight Into Terrain (CFIT). [1]

NASA's Aviation Safety Program investigated Synthetic Vision Systems (SVS) and one of the SVS goals is the mitigation of accidents due to CFIT by providing the pilots with advanced display technology containing information about aircraft state, guidance, navigation, surrounding terrain and traffic. The source of the terrain information for the SVS display is a DEM, a digital look-up table of the terrain heights corresponding to a set of position, coordinates (latitude, longitude). Examples of DEMs are Digital Terrain Elevation Database (DTED) levels 0, 1, and 2 and Jeppesen terrain databases. In order to be certified for a level of reliability further than advisory, all or a subset of the SVS subsystems must meet or exceed the required reliability ratings. This includes the DEM that could otherwise provide Hazardously Misleading Information (HMI) about the terrain to the pilots. To ensure that a DEM conforms to a given probability of fault-free detection (false alarm) and of missed detection, it becomes necessary to monitor the consistency of the terrain heights stored in the DEM with that of the real world.

Terrain Database Integrity Monitor

Terrain databases may have systematic faults and errors in the form of:

- Bias, due to coordinate transformation mismatch in the vertical and horizontal domains.
- Ramps in the vertical and horizontal domains.
- Random distributed errors in the vertical domain and circularly distributed random errors in the horizontal domain.

This paper concentrates on the bias errors in both the vertical and horizontal directions. The performance of the integrity monitor depends upon its capability to detect vertical biases and horizontal translations with a certain probability. The smaller the biases it can detect, the better the integrity monitor performs.

Vertical Direction Integrity Monitor

The integrity monitor scheme in the vertical direction has previously been described in [2], [3] and is based on a comparison of the DEM terrain profile with an independent terrain profile synthesized from downward looking external sensors in real time. The present scheme uses a Radar Altimeter (RA), Global Positioning System (GPS) and augmentation information from WAAS. The synthesized height measurements are formed as

$$h_{synt}(t_i) = h_{DGPS}(t_i) - h_{RA}(t_i) - l_{ar} \quad (1)$$

Where h_{DGPS} is the height above Mean Sea Level (MSL) as derived from DGPS measurements, h_{RA} is the height Above Ground Level (AGL) obtained from RA measurements and l_{ar} is the distance offset between the GPS and the RA antennas, typically the distance between the roof and the belly of the aircraft. All measurements are referenced to time t_i.

The metrics used to express the consistency or degree of agreement between the terrain database profile (henceforth called DTED profile) and the synthesized terrain profile are:

- Absolute Disparity (AD):
  $$p(t_i) = h_{synt}(t_i) - h_{DTED}(t_i) \quad (2)$$
  The absolute disparities are sensitive to bias errors. The Mean Squared Error (MSE) of the absolute disparities is given by $\frac{1}{N}\sum_{i=1}^{N} p^2(t_i)$ where N is the number of measurements.
- Successive Disparity:
  $$s(t_i) = p(t_i) - p(t_{i-1}) \quad (3)$$
  The successive disparities are formed by subtracting two consecutive absolute disparities, getting rid of constant biases in the sensor measurements. Successive disparities are sensitive to ramp errors.

- Cross Correlation: Magnitude as a measure of agreement between the DTED and synthesized terrain profiles.

This paper discusses the usefulness of the Absolute Disparity metric for consistency between the two terrain profiles. As described in [2], if an aircraft is flying at a height of at least 290 meters and a speed of no less than 60 meters/second, the absolute disparities obtained by subtracting the DTED (3" x 3" resolution) terrain profile from the synthesized terrain profile have independent gaussian noise characteristics with mean zero (assuming no biases) and a standard deviation of 18.9 meters.

Formulation and Testing of Hypothesis

The chi-square distribution plays a vital role in statistical inference and hypotheses testing. The chi-square distribution is an important special case of the gamma distribution:

$$f(x)=\begin{cases}\frac{1}{\beta^{\alpha}\Gamma(\alpha)}x^{\alpha-1}e^{-x/\beta}, x>0, \alpha>0, \beta>0 \\ 0 \qquad ,otherswise\end{cases} \tag{4}$$

with $\alpha=\frac{\nu}{2}$ and $\beta=2$, the parameter ν called the 'degrees of freedom' [4].

If $x_1, x_2, ...x_N$ is a random sample of size N taken from a normal population having a mean μ and the variance σ^2, then

$$\chi^2=\frac{\sum_i^N (x_i-\mu)^2}{\sigma^2} \tag{5}$$

is a random variable having the chi-square distribution with $\nu=N$ degrees of freedom. If the sample mean $\overline{X}$ is unknown, then

$$\chi^2=\frac{\sum_i^N (x_i-\overline{X})^2}{\sigma^2}$$

is a random variable having the chi-square distribution with $\nu=N-1$ degrees of freedom. Since the absolute disparities are assumed to be normally distributed, their squares $p^2(t_i)$ are chi-square distributed and a test statistic concerning p^2 shall be formulated later in this section.

The basic steps to be followed for any hypotheses testing are reproduced here from [4].

1. Formulate a Null Hypothesis (H_0) and an appropriate Alternate Hypothesis (H_1) that is accepted when the Null Hypothesis must be rejected.
2. Specify the probability of a Type I error for H_0; if necessary, also specify the probability of a Type II error for H_1.
3. Based on the sampling distribution of an appropriate statistic, construct a criterion for testing the null hypothesis against the given alternative hypothesis.
4. Calculate from the data, the value of the statistic on which the decision is to be based.
5. Decide whether to reject the null hypothesis, accept it or to reserve judgment.

Rejection of hypothesis H_0 when it is true is referred to as either a Type I error or a fault-free detection or false alarm. Acceptance of hypothesis H_0 when it is false is referred to as Type II error or a missed detection.

Table 1. Decision Making in Hypothesis Testing

	Accept H_0	**Reject H_0**
H_0 is true	Correct Decision	Type I error (Fault-free Detection)
H_0 is false	Type II error (Missed Detection)	Correct Decision

The metrics used to perform hypothesis testing are random variables with a probability distribution due to the inherent presence of measurement noise on the sensors (RA, GPS positions), vertical and horizontal error probability specification of the DEM, random errors on the DEM and ground cover (vegetation). Thus, the integrity metrics must be characterized statistically.

Under the fault-free condition (no bias), the over-bound of the probability density of the errors

on the sensors and the DEM yields a normal probability density function (PDF), which leads to the following null hypothesis or fault-free hypothesis:

$$\mathrm{H}_0 : p_0 \sim N\left(0, \sigma_p^2\right) \tag{6}$$

where $N\left(0, \sigma_p^2\right)$ is a normal distribution with mean zero and variance σ_p^2. The variance σ_p^2 is derived from the convolved variances of the individual sensor error PDFs, errors due to ground cover and the specified error characteristics of the DEM [2].

When a failure mode exists in the form of a bias on either the sensors or the DEM or both, the bias shows up in the PDF of the absolute disparities as the mean, giving rise to the alternate or faulted hypothesis:

$$\mathrm{H}_1 : p_1 \sim N\left(\mu, \sigma_p^2\right) \tag{7}$$

where μ is the failure bias. [3] furthermore defines a minimum detectable bias, μ_B as the smallest bias that can be detected with a probability of 1- P_{MD}.

Forming the chi-square statistic as in equation (5) by scaling the sum of squares of the ADs by the variance of the noise on the ADs under nominal conditions gives rise to the Test Statistic, *T*:

$$T = \frac{1}{\sigma_p^2} \sum_{i=1}^{N} p^2\left(t_i\right) \tag{8}$$

Under H_0, *T* is chi-square distributed with N degrees of freedom and under H_1, *T* is non-central chi-square distributed with *N* degrees of freedom and non-centrality parameter λ [5]. Figure 1 shows a representation of the distributions of the test statistic, *T*, under H_0 and H_1 hypotheses [3].

For the purpose of this paper, the probability of fault-free detection (P_{FFD}, Type I error) is taken as 10^{-4} and the probability of missed detection (P_{MD}, Type II error) is specified as 10^{-7}.

For the given P_{FFD} and $N = 50$ successive measurements (degrees of freedom is equal to the number of measurements), the threshold value of the chi-square statistic '*T*', on which the decision has to be based can be looked up from the chi-square distribution tables or calculated from equation (4). Figure 2. shows a look-up plot for the threshold values for various degrees of freedom and various P_{FFD}, the values having been generated using [6].

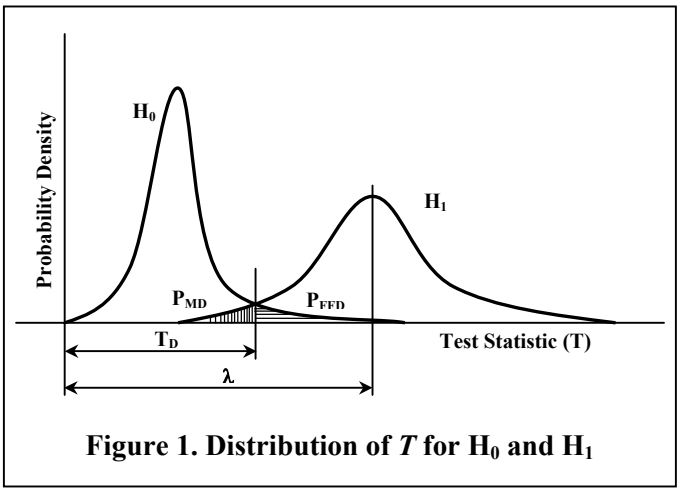

Figure 1. Distribution of *T* for H_0 and H_1

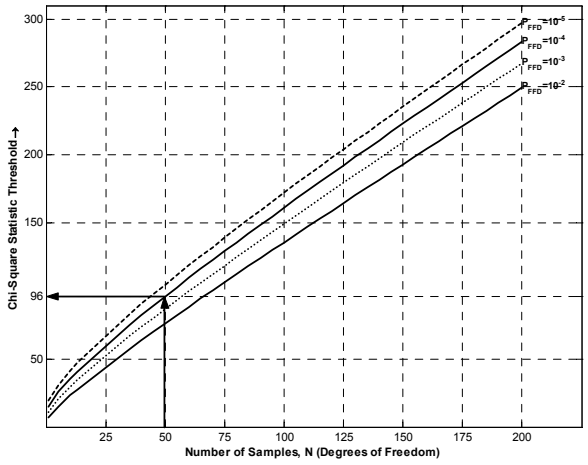

Figure 2. Threshold value for chi-square statistic

For $P_{FFD} = 10^{-4}$ and $N = 50$, the test statistic threshold (T_D) was found to be 96. A look-up graph to find the value of the non-centrality parameter λ, given a P_{MD} and the threshold value of the test statistic is given in Figure 3, the values having been generated using [6].

For $P_{MD} = 10^{-7}$, $T_D = 96$ and $N = 50$, λ is found to be 164.17. Assuming a constant minimum detectable bias μ_B on the disparities, the non-centrality parameter λ is related to the bias error [5]

$$\lambda = \frac{N}{\sigma_p^2} \mu_B^2 \tag{9}$$

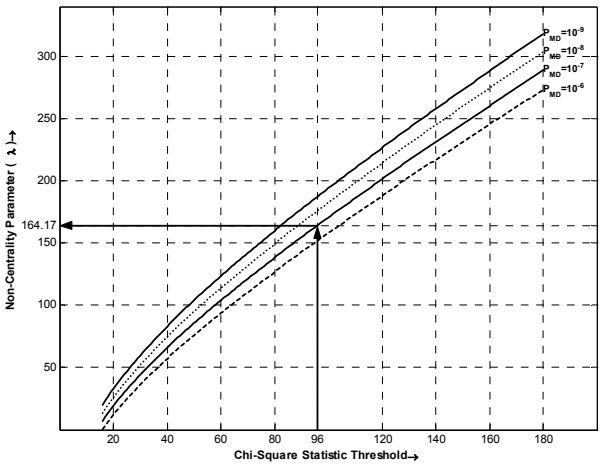

Figure 3. Non-Centrality parameter look-up plot

Using equation (9) and $\sigma_p^2 = (18.9)^2$, the variance of the total noise on the absolute disparities as calculated in [2], μ_B is found to be equal to 34.2 meters, i.e. H_0 is rejected with a probability of 1-P_{MD} if a bias of 34.2 meters or more exists. This is shown to be true by a Monte Carlo analysis in the next section.

Error Analysis

A Monte Carlo analysis with 10000 simulations was performed using MATLAB™, generating normally distributed pseudo-random numbers with mean varying from 0 to 50 m and $\sigma_P = 18.9m$. The T value was calculated for each run and compared to threshold, T_D. The results are shown in Figure 4 as the probability of accepting H_0 under the presence of a bias, μ.

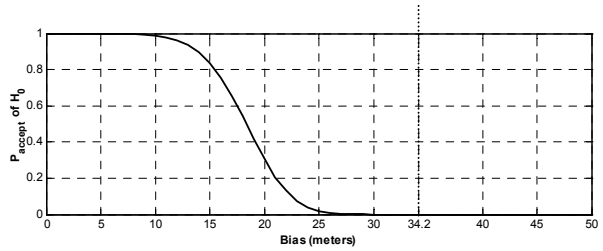

Figure 4. Operating Characteristics (OC) Curve

The OC curve shows the probability of accepting the null hypothesis under the presence of a bias fault. This probability decreases as the bias increases and at a bias of 34.2m and above, the null hypothesis is accepted only with a probability of less than 10^{-7}.

Flight Test Results

Ideally, $p(t_i)$ equals zero but due to noise on the DEM and sensors, the variance of $p(t_i)$ is $(18.9)^2$. In case of the presence of biases on the sensors and DEM, the absolute disparities are given by

$$p = noise_{sensors+DEM} + bias_{sensors+DEM}$$

Since we are looking for regions of zero bias, we model the AD as being zero mean gaussian with $\sigma^2 = (18.9)^2$. Therefore, $T = \dfrac{\sum_{i=1}^{50} p_i^2}{(18.9)^2}$

Figure 5 shows the computed values of the T statistic for various approaches to runway 25 during NASA's flight tests at Eagle county (EGE), CO using their Boeing 757 ARIES test aircraft in 2001. The first plot is for zero bias and the next two are for deliberately introduced biases of 25m and 35m respectively.

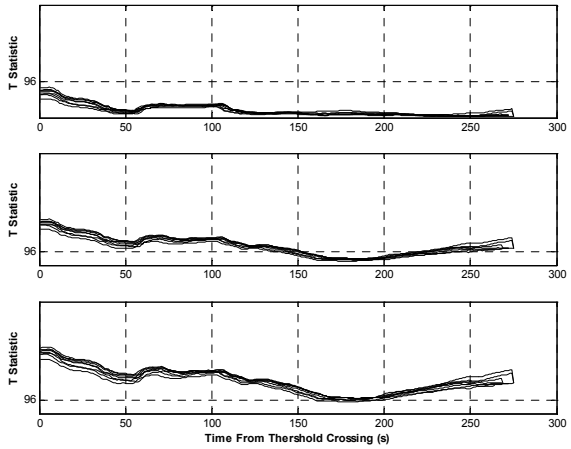

Figure 5. T value during approach to R/W 25 at EGE for biases of 0m, 25m and 35m.

The plots show clearly that for a bias of 25 meters (less than MDB), only a few points exceed the threshold of 96, whereas for a bias of 35 meters, most of the points exceed the threshold of 96, thus forcing us to reject the null hypothesis H_0 and provide the pilots with an aural or visual alert.

Horizontal Direction Integrity Monitor

So far, the terrain database integrity monitor focused on the detection of faults in the vertical direction. One horizontal direction integrity monitor concept was introduced in [3] referred to as the Multiple Path Downward Looking Integrity Monitor (MPDLIM). The concept is based on computing the *T* statistic for multiple flight paths parallel to the nominal flight path (given by GPS positions) over a rectangular search grid. The *T* value at each point over the grid gives a measure of similarity between the DEM terrain profiles within the search area and the synthesized terrain profile. In essence, the vertical direction integrity monitor has been extended so that multiple terrain profiles from the DEM would be compared to a single synthesized terrain profile, and all the grid points that do not exceed the chi-square distribution threshold are probable aircraft positions. The region formed by all such points is referred to as the 'region of missed detection'.

The expression for the test statistic *T*, can symbolically be written as:

$$T(m,n) = \frac{1}{\sigma^2}\sum_{i=1}^{N}\left(h_{SYNT}(t_i) - h_{DTED}(x,y)\right)^2 \qquad (10)$$

where

$$x = lat(t_i) + lat\_offset_m \quad for \quad m = -P \quad to \quad P$$

$$y = lon(t_i) + lon\_offset_n \quad for \quad n = -P \quad to \quad P$$

It should be mentioned that the performance of such a horizontal direction integrity monitor is a function of the terrain signature (roughness and non-periodicity). The performance relies greatly on the deviation of the DEM terrain profile from the synthesized profile over the different points in the search grid. For terrain with a large spatial similarity such as flat or periodic terrain, the computed *T* values are similar over the entire search grid, resulting in a decreased MPDLIM performance. However, while traversing such terrain, the CFIT risk is in general much smaller. Rough, quick-varying and non-periodic terrain offers improved performance of the horizontal integrity monitor as well as increased risk of CFIT. A measure of the terrain roughness can be obtained from the average size of the terrain gradient, called the information content of the terrain [7]:

$$I = \sqrt{\frac{1}{N}\sum_{i=2}^{N}\left(\Delta h_{synth}\right)^2} \qquad (11)$$

Terrain elevation plots and regions of missed detection are shown in Figure 6 for an approach to runway 25 at EGE (6a) and at JNU (6d)

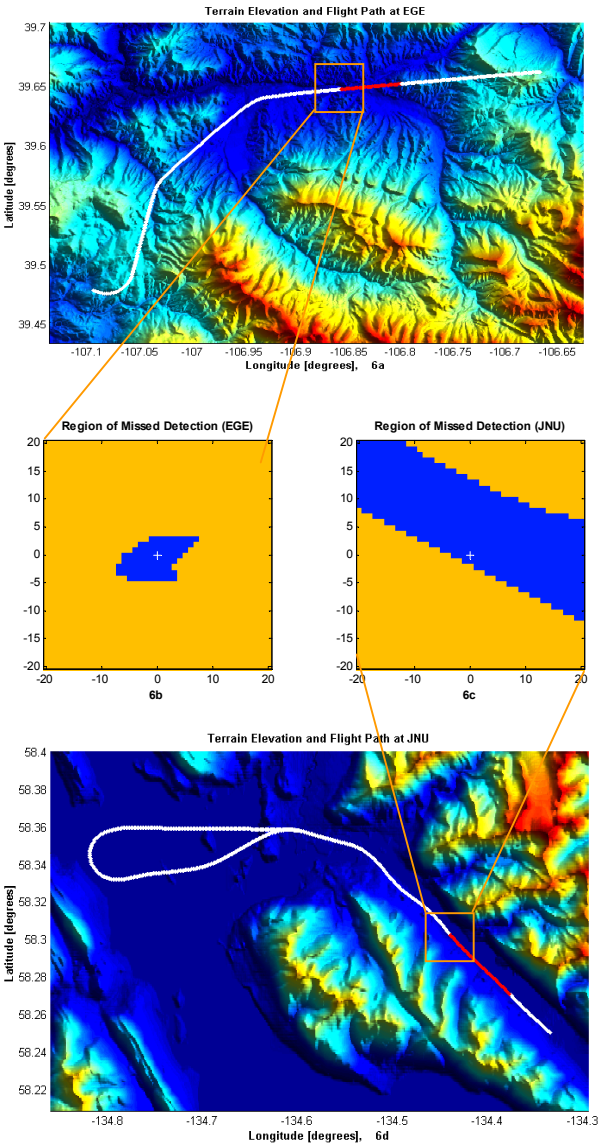

Figure 6. Region of Missed Detection within –20 to 20 resolution grid in latitude and longitude.

The dark areas in figures 6b and 6c represent the regions of missed detection. The difference in the horizontal translation detection capability at

EGE and JNU can directly be related to the terrain signature at both the locations (given by equation (11)). Flying through the Gastinuea channel near JNU shows a poor along-track detection performance due to the lack of terrain undulations along the aircraft's track. However, the cross-track detection performance is better due to the presence of mountains on either side of the channel. Note that the along-track CFIT risk is also much smaller than the cross-track CFIT risk. The high terrain information content at EGE, on the other hand, provides a smaller region of missed detection.

Improved Detection Using Kalman Filter

A Kalman filter could be used on the absolute disparities to reduce the nominal noise (sensors + DEM) and estimate a potential bias error (sensors + DEM). If the errors are Gaussian, the Kalman filter is an optimal estimator of the bias error in the Minimum Mean Squared Error (MMSE) sense. The system model is given by a bias plus noise or $z = \mu + n$ where *n* is zero mean gaussian noise with a standard deviation of 18.9 meters. The Kalman filter equations are reproduced from [8], and an explanation of the matrix terms given.

1. Specify initial prediction $\hat{x}_0^-$ and its error variance P_0^-.
2. Compute Kalman filter gain:
   $$K_k = P_k^- H_k^T \left(H_k P_k^- H_k^T + R_k \right)^{-1}$$
3. Update estimate with measurement:
   $$\hat{x}_k = \hat{x}_k^- + K_k \left(z_k - H_k \hat{x}_k^- \right)$$
4. Compute estimation error variance:
   $$P_k = \left(I - K_k H_k \right) P_k^-$$
5. Project ahead
   $$\hat{x}_{k+1}^- = \phi_k \hat{x}_k$$
   $$P_{k+1}^- = \phi_k P_k \phi_k^T + Q_k$$
6. ←

where:

$\hat{x}_0^-$ is zero as per the assumed system model,

P_0^- is $(19.83)^2$ assuming one σ (68%) prediction error variance,

ϕ_k is the state transition matrix; unity,

z_k is the measurement at time t_k; absolute disparities,

H_k is the domain transition matrix; unity,

P_k is the estimation error variance at time t_k,

R_k is the measurement error variance; the variance on the absolute disparities $(18.9)^2$, constant,

Q_k is the system noise variance or also called the tuning parameter of the filter (also a constant).

Based on this tuning parameter *Q*, the variance of the estimates, *P*, attains a constant steady-state value over time. If the aircraft were to be flown so as to cover the entire area of the DEM, and the filter is let to run for all the absolute disparities, *P* would be the variance of the complete population of filtered estimates over the area of the DEM. Thus the *T*-value using the filtered estimates can be computed as:

$$T = \frac{1}{P} \sum_{k=1}^{N} \hat{x}^2 \left(t_k \right) \tag{12}$$

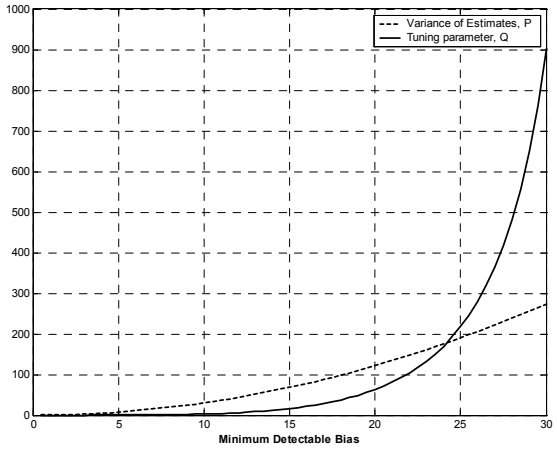

Figure 7. *P* and *Q* as a function of μ_B.

Now, an interesting deduction stems from the above argument that Q can be varied such that P settles at a certain steady-state value and substituting σ_P^2 by P in equation (9), the MDB μ_B for the Kalman filtered case can be computed. Or, working backwards, for a desired value of μ_B, the variance of estimates P and hence the tuning parameter Q can be calculated. Figure 7 shows a plot of both P and Q as a function of μ_B.

The Cramer-Rao lower bound on the variance of the estimates is the variance of the ordinary least squares filter, i.e. $\sigma_P^2 / N = 7.14$ and a lower bound on μ_B is found to be equal to 4.84 meters by substituting the Cramer-Rao lower bound on the variance into equation (9).

However, filtering of the absolute disparities violates the basic assumption of equations (5) and (8) that the underlying random variables, x_i, are independent; equations (5) and (8) are only valid for independent samples taken from a normal distribution. The filtered estimates are no longer independent but are highly correlated and equation (12) no longer applies in a strict sense. The amount of correlation of the estimates, in time, depends upon the tuning parameter of the filter, Q. It turns out that for relatively larger values Q (and thus μ_B), equation (12) can still be used to a certain extent without much damage done to the pre-specified P_{FFD} and P_{MD} as shown in the next section.

Error Analysis Revisited

A Monte Carlo analysis with 10000 simulations was performed and the autocorrelation functions of unfiltered gaussian noise, Kalman filter estimates for minimum detectable bias of 25 meters and 15 meters have been plotted. Figure 8 shows that decreasing the minimum detectable bias and hence the tuning parameter Q results in an increase of the sample correlation time. The same notion is conveyed by the correlation coefficients as a function of time difference between samples in figure 9.

The de-correlation time of the Kalman estimates for μ_B of 25 meters is about 5 seconds whereas for μ_B of 15 meters is much longer.

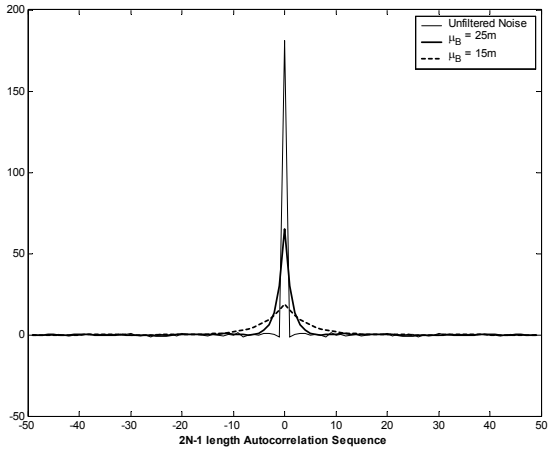

Figure 8. Autocorrelation sequence of Kalman estimates for μ_B of 34.2m, 25m and 15m.

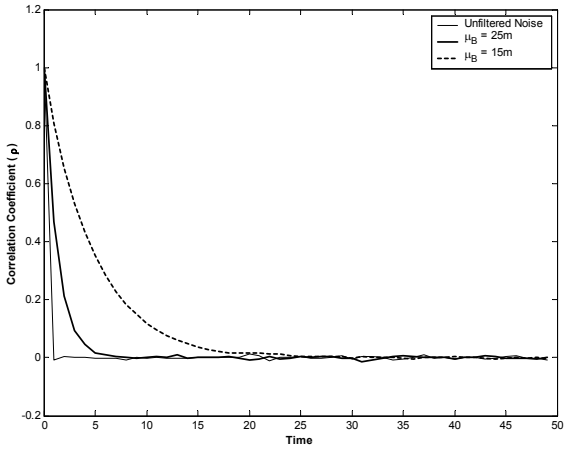

Figure 9. Correlation Coefficient (ρ) of Kalman estimates for μ_B of 34.2m, 25m and 15m.

In the former case, to obtain independent samples, one must pick the estimates every 5 seconds. This would reduce the degrees of freedom in equation (5) by a factor of 5. Maintaining the same amount of degrees of freedom could be achieved by increasing the number of original samples. However, this would increase the time-to-alert by a factor of 5 also.

Considering these arguments, one must look for an acceptable amount of deviation from strict theory. The operating characteristics curves for the three cases discussed are shown in figure 10. Even though the filter is set up for a μ_B of 15 meters, there is still a probability of accepting the null hypothesis. This probability, from figure 10 is quite

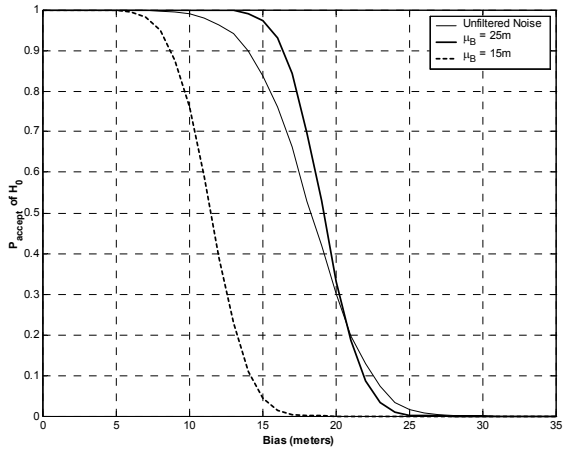

Figure 10. OC Curve of Kalman estimates for μ_B of 34.2m, 25m and 15m.

large compared to the P_{FFD} and P_{MD}. The OC curve for μ_B of 25 meters looks encouraging, with the probability of accepting H_0 becoming very small.

Flight Test Results With Kalman Filtering

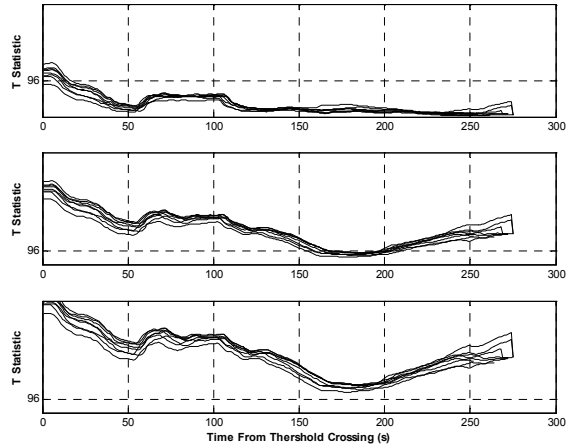

Figure 11. T statistic during approach to R/W 25 at EGE for biases of 0m, 25m and 35m.

Figure 11 shows the *T*-values for a Kalman filter aided vertical direction integrity monitor. Comparison with Figure 5 shows an improved detection capability for higher biases. In order to allow the filter to settle down to steady state, henceforth, 60 seconds of absolute disparities are run through the Kalman filter and the last 50 seconds of estimates used to compute the *T* statistic.

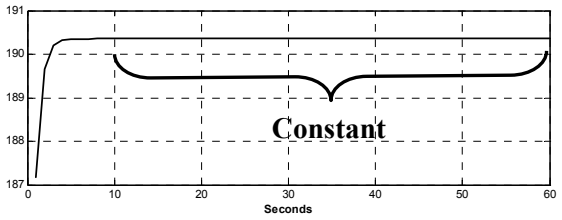

Figure 12. Kalman estimation error variance

An improvement in the horizontal detection capability of the integrity monitor is shown in figure 13. The smaller the region of missed detection, the better the performance of the integrity monitor.

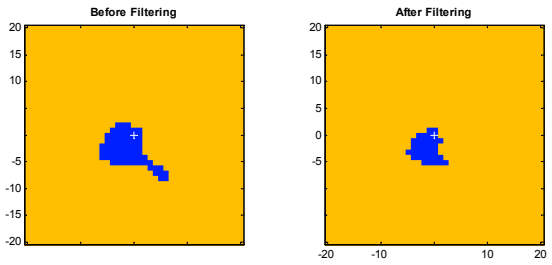

Figure 13. Region of missed detection during approach to R/W 25 at EGE

In figure 13, the '+' sign gives the GPS position considered to be the truth and the dark areas are probable aircraft positions (according to the DEM) that fail to generate an integrity alarm.

Figures 14a, b show the areas of missed detection computed over the entire flight path superimposed upon the terrain features and true GPS positions. Figure 14b shows a reduction in the region of missed detection over 14a. The dark areas in the figures are valleys that have smaller terrain information content and thus a larger area of missed detection than the rocky mountainous regions. There are also a few seconds during the flight when the filtered case does not have any area of missed detection i.e. the *T* value exceeds the threshold at all locations within the search grid for these time epochs. This happens just after the aircraft turns and can be attributed to a deviation of the radar altimeter measurement from it's nominal performance; the radar altimeters measure the slant height instead of the 'plumb-bob' height and the

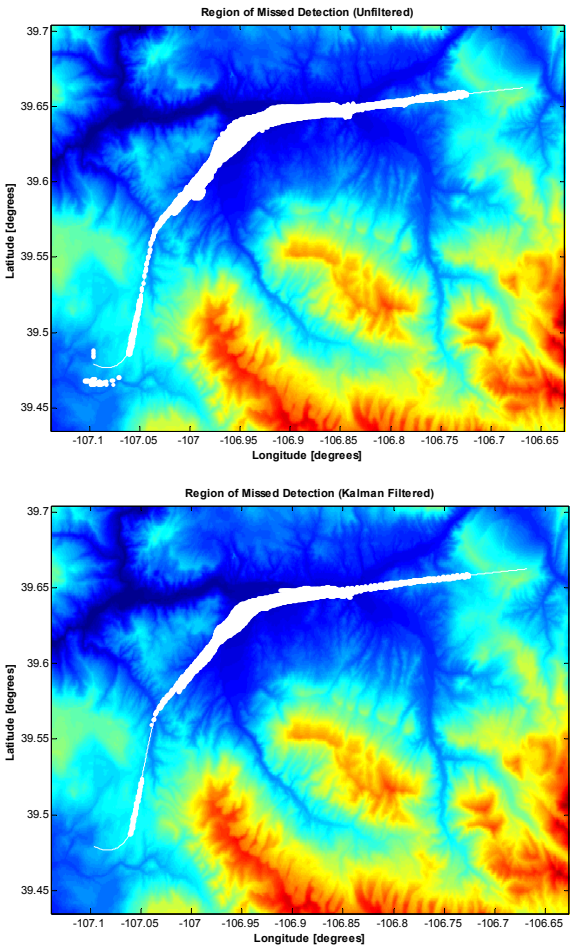

Figure 14a,b. Region of missed detection during entire flight path at EGE

Kalman filter's characteristic of storing past history makes the effect of bad data points conspicuous after a few seconds.

Having discussed both vertical and horizontal direction terrain database integrity monitors, it is possible to combine the two in order to form a spatial failure mode detector/integrity monitor. The idea is to introduce vertical biases and use the horizontal integrity monitor concept at each vertical bias to form a volume or 'space envelope' of missed detection.

The star '*' in figures 15a and 15b represents the GPS aircraft positions and the space envelopes have been plotted as contour maps. At first glance, the space envelopes seem to be violating the results proved earlier on minimum detectable biases, but actually, the contours that extend beyond 35m and 25m in figures 15a and 15b respectively do not include the horizontal grid points lying directly below the actual GPS positions.

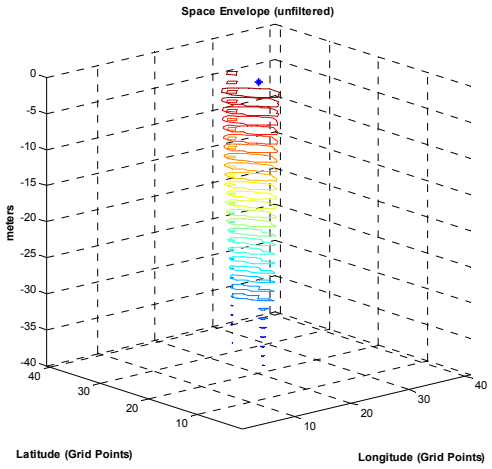

Figure 15a. Space Envelope without filtering.

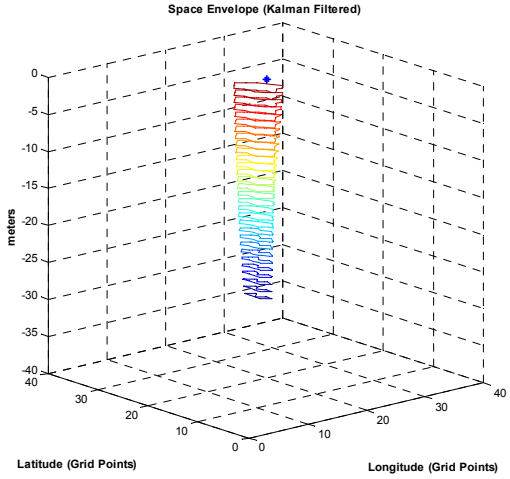

Figure 15b. Kalman filtered Space Envelope.

Terrain Navigation

The *T* value can also be used for Terrain Navigation, also known as Map-aided navigation. Since the *T* value is a measure of the agreement between the synthesized terrain profile and the DEM terrain profile, a minimum *T* implies maximum agreement between the two terrain profiles. The figures 16a and 16b depict the minimum *T* positions computed at every 5-second intervals of the flight path for an approach to runway 7 at EGE. The trajectory of the minimum *T* positions closely follows the GPS positions except

in regions just after a sharp turn. This error is caused by a systematic error in the radar altimeter during large bank angles that causes the synthesized height to be not representative of the terrain database height [3]. Figures 16a and 16b are quite similar to each other, but the filtered case is less sensitive to radar altimeter measurement error due to the aircraft's banking maneuver by modeling the slant height measurement as a pseudo-bias.

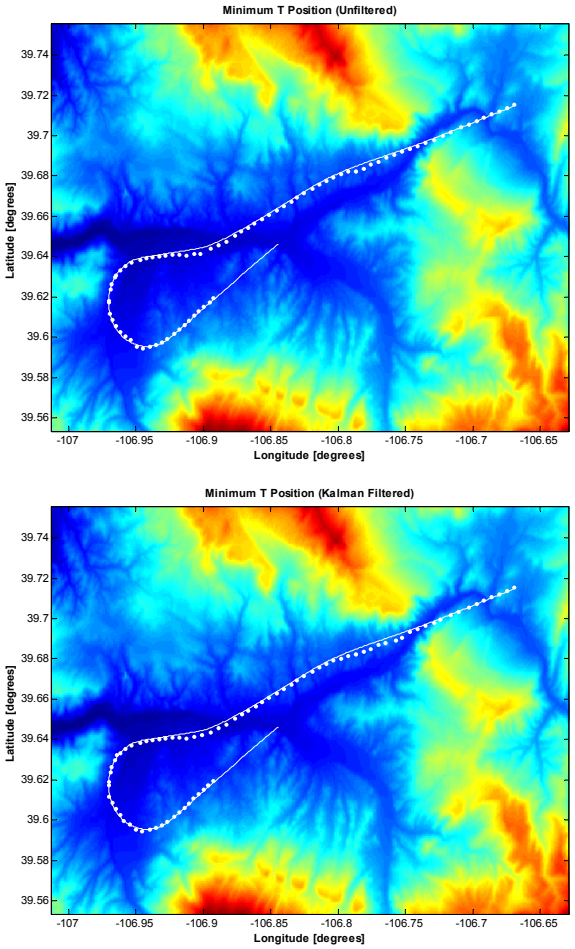

Figure 16a (upper) and 16b (lower). Minimum T positions for Terrain Navigation

A plot of the minimum *T* positions collapsed onto a single grid is shown in figure 17. All minimum values cluster around the GPS position value (grid co-ordinates of (0,0)) showing no horizontal bias. When a 30"x30" bias was introduced in the DEM, the cluster of the minimum *T* positions translates accordingly, thus proving the capability of detecting horizontal biases and making navigation decisions.

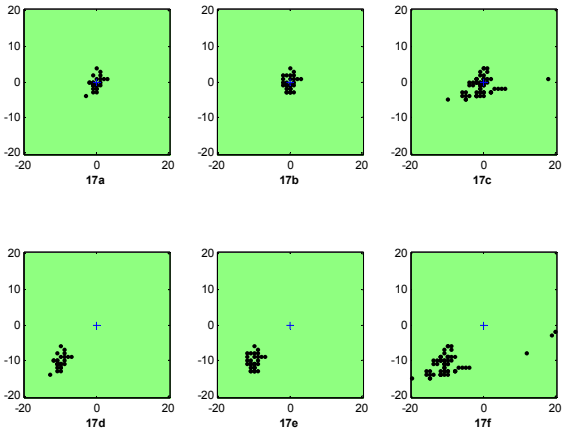

Figure 17. Detecting horizontal translation in the DEM

Figure 17a, 17b and 17c are the unfiltered, Kalman filtered and Least Squares filtered cases respectively, the example of ordinary least squared filtering provided for comparison. 17d, 17e and 17f are the figures corresponding to the previous ones with the horizontal bias included.

Summary and Conclusions

Terrain database integrity monitors might be necessary for SVS to enable them to meet integrity requirements more stringent than advisory. Statistical characterization of the vertical direction integrity monitor with regard to its minimum detectable bias is straightforward, but statistical characterization of the horizontal detection capability is more challenging. That the vertical bias would not exceed the MDB is a great assurance but the same cannot be said of the horizontal direction. Data from two flight tests at places of highly contrasting terrain features, one at Eagle/Vail, Colorado in the vicinity of the Rocky Mountains, and another at Juneau, Alaska, close to icy glaciers was used to study the performance of the horizontal direction integrity monitor. The results confirm the theoretical understanding that the horizontal fault detection capability is dependent upon the information content offered by the terrain.

The Kalman filter improves the statistical detection capability for terrain database integrity monitoring for both vertical biases and horizontal translations. As is the case with any filtering

operation, the Kalman filter alters the statistical properties of the system model. An analysis of the effects of filtering has been carried out with a reliability point of view and the involved tradeoffs between strict theory and practical applicability have been discussed.

Applicability of filtering techniques for terrain navigation using the test statistic approach has been explored. The minimum T-value point on the search grid gives the most likely DEM position of the aircraft. Position estimates formed using the Kalman filtered absolute disparities are much closer to the GPS positions during banking phases of flight than unfiltered absolute disparities. The positions thus obtained could be used for *en-route* navigation with an acceptable horizontal translation error that depends upon the terrain signature. More precise DEM position estimates require closer spacing of the search grid points which in turn requires a higher resolution DEM.

Though the Kalman filtering approach to integrity monitoring yields promising results, a thorough study of the relation between horizontal detection capability and terrain signature is recommended. This might involve a higher quality DEM and in-depth research to quantify the terrain features and relate them to a minimum detectable horizontal bias.

References

[1] Williams, D., et al., January 2001, "Concept of Operations for Commercial and Business Aircraft Synthetic Vision Systems – Version1.0," NASA Langley Research Center.

[2] Gray, R.A., 1999, "Inflight Detection of Errors for Enhanced Aircraft Flight Safety and Vertical Accuracy Improvement using Digital Terrain Elevation Data With an Inertial Navigation System, Global Positioning System and Radar Altimeter", Ph.D. Dissertation, Department of Electrical and Computer Engineering, Ohio University, Athens, Ohio, ch. 3,7.

[3] Campbell, J., November 2001, "Characteristics of a real-time digital terrain database integrity monitor for a synthetic vision system", MS thesis, Department of Electrical and Computer Engineering, Ohio University, Athens, Ohio, ch. 2.

[4] Johnson, R.A., 1995 "Miller and Freund's Probability and Statistics for Engineers", fifth edition, Prentice Hall.

[5] Uijt de Haag, M. et al., April 16, 2001, "Flight Test Results of a Synthetic Vision Elevation Database Integrity Monitor", Orlando, Fl, Proceedings of the Society of Photo-Optical Instrumentation Engineers (SPIE).

[6] http://calculators.stat.ucla.edu/cdf/

[7] Bergman, N., L. Ljung and F. Gustafsson, June 1999, "Terrain Navigation using Bayesian Statistics", IEEE Control Systems Journal, pp. 34.

[8] Brown, R. G and P. Y. C. Hwang, 1997, "Introduction to Random Signals and Applied Kalman Filtering", John Wiley & Sons.